ATLAS

FUNDAMENTAL TECHNIQUES, MODELS AND ALGORITHMS FOR A LUNAR RADIO NAVIGATION SYSTEM

ESA AO/1-10712/21/NL/CRS

Executive summary

Reference: CRAS/2021/ATLAS_ES-001

Sapienza Aerospace Research Centre – CRAS
Sapienza Università di Roma
Via Eudossiana 18, 00184, Rome, Italy

Centre National de Recherche Scientifique
CNRS delegation Côte d'Azur
Campus Azur 250 av. A. Einstein, Bat3 CS 10269
06905 Sophia Antipolis Cedex, France

Institute of Geodesy and Geoinformatics
Wrocław University of Environmental and Life Sciences
Norwida 25, 50-375 Wrocław, Poland

Argotec S.r.l.
Via Cervino, 52, IT-10155, Turin, Italy

Leonardo S.p.A.
Viale Europa snc, IT-20014, Nerviano (MI), Italy

1 OVERVIEW

This document outlines the global architecture proposed by the ATLAS consortium and the main results of our analysis, in response to the Statement of Work (SOW) of the AO/1-10712/21/NL/CRS.

The documentation delivered consists of:

1) Concept Document - Part 1 (CD-1)
2) Concept Document – Part 2 (CD-2)
3) Annex to Concept Document (CD-Annex-A)
4) Annex to Concept Document (CD-Annex-B)
5) Concept Requirement Document (CRD)
6) Service Definition Document (SDD)
7) Technology Roadmap (TR)
8) Simulation Software: Orbit Determination and Time Synchronization (SS-OD+TS)
9) SS-OD+TS User Manual (SS-UM)

In **CD-1** we addressed the architecture and rationale of the requirements for a lunar radio navigation system (LRNS) able to support future positioning and navigation needs of end users in the lunar environment. CD-1 focusses on the ODTS and reference frames, with the description of an architecture aimed at meeting the SOW requirements. **CD-2** describes the LRNS signals and the navigation message. **CD-Annex-A** reports on the analysis of an architecture based on sequential tracking. This architecture was abandoned during the study, due to its clearly inferior performances. **CD-Annex-B** reports on our analysis for reference frames and time scales in a relativistic context, for possible use by Moonlight. The **CRD** presents a list of high-level requirements needed to successfully implement the LRNS architecture proposed by the ATLAS consortium and described in CD-1 and CD-2. The **SDD** describes the characteristics and performance of the LRNS ODTS provided through the LRNS signal-in-space (SIS), and reports on the performances that the proposed service can provide to the constellation in terms of minimum levels. The **TR** identifies the TRL of the key elements of the ATLAS architecture (as presented also in CD-1) and outlines a roadmap for the needed technology developments. **SS-OD+TS** is a full software simulator based on the GODOT orbit determination (OD) software package (developed at ESOC). The simulator has been used to run and analyse all test cases concerning OD and time synchronization (TS). The simulator has been delivered to ESA via Gitlab and is accompanied by a user manual (**SS-UM**).

A key feature of the ATLAS ODTS architecture is a ground segment based on a network of ground antennas that simultaneously track all satellites in the constellation using K-band frequency links. The multiple spacecraft per aperture (MSPA) configuration ensures sufficient data rates and achieves high accuracy in Doppler and range observables, enabling precise orbit determination. One notable outcome of MSPA is the availability of a new observable quantity, the differential phase of the two-way signals received by the ground station from any pair of satellites, also known as single-beam interferometry (SBI). For time transfer and synchronization, we considered with different onboard clocks and evaluated the accuracies of the standard asynchronous two-way satellite time and frequency transfer (TWSTFT) method, as well as those of a novel time transfer method, leveraging onboard code epoch timestamping and precise spacecraft range information. Through the analysis of realistic test cases, the study demonstrates that orbit determination accuracies consistently remain below 10 meters (root sum square). Furthermore, the findings indicate that ephemerides aging and clock drifts align well with a navigation message repeat time of approximately three hours (99% confidence level), while maintaining a signal-in-space error (SISE) of 25 meters.

The most promising time scales of the constellation and their relation to TT and TCB were analyzed in a relativistic context. The two possible choices for the lunar, body-fixed reference frame (Mean Earth – ME – and Principal Axes – PA) were reviewed. Although the final choice for time scales and reference frames will be made by the NASA-ESA coordination group and, ultimately, the IAU, the ATLAS team offered support to ESA in the discussions (still ongoing) with NASA. CD-1 presents the pros and cons of a lunar time scale (LTS) vs. the use of TT/TAI.

2 RADIO SYSTEM ARCHITECTURE

The radio system architecture for the Telemetry, Tracking and Command (TT&C) of the constellation during nominal operations, as well as for OD and time synchronization (TS), hinges on two main design choices, driving LNCS performance, signal structure definition, and ground and onboard hardware.

The first is the use of K-band for uplink and downlink signals, offering numerous advantages compared to X band. The most obvious is the larger available bandwidth (500 MHz overall, compared to 50 MHz at X-band), allowing for higher code chip rate in spread spectrum (SS) modulation and increased accuracies of range measurements and time transfer. K-band is also much less affected by ionospheric delays. Yet, the strongest advantage of K-band lies in the expandability of the constellation, which is problematic in the congested X-band.

The second design choice concerns the use of the code division multiplexing scheme (CDM) based on SS modulation, which enables allocating the same frequency band to the four satellites of the constellation with consequent saving of spectral resources, at the expense of additional design complexity for the ground station modem and the onboard transponder. Furthermore, if the CDM technique is implemented in a multiple spacecraft per aperture (MSPA) scheme, it is possible to track, control and synchronize the entire constellation simultaneously by implementing nearly continuous TT&C operations and parallelizing OD and time transfer (TT) functions (figure 1). Since MSPA requires the constellation to be within the main lobe of the ground antenna, the constellation geometry drives the maximum size of the ground terminal. A pointing strategy based on the minimum enclosing circle curtails most pointing losses. Analyses show that a Half Power Beamwidth (HPBW) of about 3 degrees guarantees a 99% visibility for the full constellation, corresponding to a dish diameter of 26 cm at K-band. Though small antennas are inexpensive and easily maintained, they are also more exposed to radiation disturbances from the surrounding environment, necessitating a resilient signal structure, as presented in the upcoming section. It is however well known that SS receivers have intrinsic interference rejection properties and the longer are the SS sequences, the better is the interference suppression. Electromagnetically clean sites for the ground stations are anyway recommended.

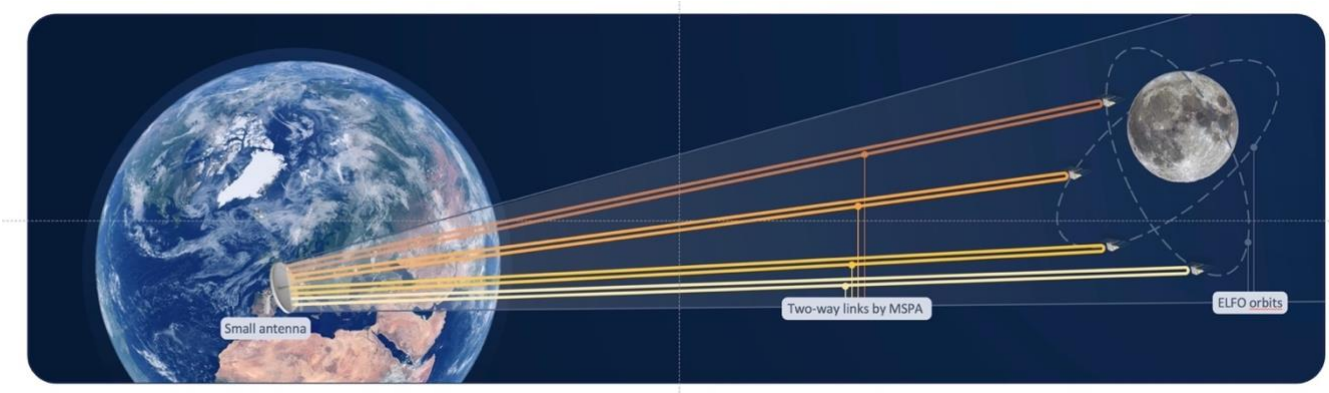

FIGURE 1 MSPA architecture, showcasing the capability to perform simultaneously TT&C operations, acquisition of Doppler, range, and SBI measurement, and TT for all four spacecraft of the constellation.

Signal Structure. SS modulation represents the backbone of any GNSS as it enables simultaneous signal transmission, better time-delay resolution, as well as good immunity to interferences, especially for long SS sequences (Meurer & Antreich, 2017). The ground station transmits 24 Mcps SS signals with a modulation format derived from (CCSDS, 2011). The modulation is offset quadrature phase shift keying (OQPSK) with a CDM scheme, where the four SS streams associated with the I-Channel are superimposed and then fed to the majority

vote logic (CDM-M) used to generate a constant envelope Binary Phase Shift Keying (BPSK) signal, suitable for operations in non-linear channels.

The four codes of the I-channel are short Gold codes (210-1 chips length) used also for on-board carrier signal acquisition. The Q-channel code (same for all four satellites) is a truncated maximum length (TML) sequence generated by a linear feedback shift register with N=18. The TML sequence has a length of 256 times the length of the Gold code [256(210-1) chips] and is synchronous with it. This feature is used by the on-board transponder to aid the acquisition of the long TML sequence. After the on-board signal acquisition, the ground station can send telecommand data on the relevant I-channel component.

The four codes of the I-channel are short Gold codes (210-1 chips length) used also for on-board carrier signal acquisition. The Q-channel code (same for all four satellites) is a truncated maximum length (TML) sequence generated by a linear feedback shift register with N=18. The TML sequence has a length of 256 times the length of the Gold code [256(210-1) chips] and is synchronous with it. This feature is used by the on-board transponder to aid the acquisition of the long TML sequence. After the on-board signal acquisition, the ground station can send telecommand data on the relevant I-channel component.

The return link signal generated by the on-board transponder is different depending on the transponder configuration (table 1), i.e.: coherent or non-coherent mode. In non-coherent mode, short Gold codes are transmitted to simplify the implementation of the SS acquisition algorithm at the ground station, and acquire the relevant QPSK telemetry. In coherent mode, two TML sequences (of the same family as the received one) are transmitted in the I- and Q-channels. The two TML sequences are synchronized in terms of both chip rates and code epochs (CE). By doing so the ground station modem can acquire the long TML sequences aiding the SS code search with the preliminary knowledge of the spacecraft distance, and the associated turn-around delay. The TML sequences turn-around in coherent mode allows the ranging, Doppler and CE measurements to occur, parallelizing OD & TS functions. Finally, QPSK modulation enables a balanced I and Q modulation format (telemetry data both on I and Q component).

In particular mission phases, for instance during contingencies, the TT&C link can be configured with PCM/PSK/PM standards (CCSDS 2021), which significantly widens the ground support beyond the stations dedicated to the LRNS. The satellite in contingency is contacted by a dedicated ground station equipped with a high directivity (and power) antenna to close the link via an onboard low gain antenna (LGA). Although the interference between the standard-modulated signal (for the contingent satellite) and the SS signals (for the nominal satellites) shall be kept under control, the power unbalance favours the former, which, coupled with the limited interference suppression capability of short Gold codes, suggests the use of mitigation strategies. The first is to employ a different frequency channel for the contingency mode. This would require a frequency-flexible transponder, a feature that could also facilitate simultaneous launches by leveraging on external ground stations supporting only CCSDS standard modulation during the launch and early orbit phase (LEOP). Alternatively, a proper filtering mechanism in the SS acquisition/demodulation processing could be implemented to suppress the standard signal interference, as proposed by Simone et al. (2010), where an adaptive cancellation algorithm was analysed for jamming rejection in SS receivers.

A detailed analysis of the Earth-Moon signal structure is reported in CD-2, where we addressed: The TT&C preliminary and generic requirements; The TT&C requirements for SS modulation; The TT&C requirements for time and frequency transfer; The Requirement vs technology; The link dynamics(Doppler & Doppler rate.

Onboard Radio System. Figure 2 shows the proposed architecture for the onboard radio system, which consists of:

- One 30 cm steerable, two degrees of freedom, medium gain antenna (MGA) for nominal operations
- Two LGA for quasi-omnidirectional coverage when the MGA is not available (as in LEOP or contingency phases)
- Two redundant K-band dual-mode transponders (hot redundancy for the RX and cold redundancy for the TX)
- Two traveling-wave-tube amplifiers (10W TWTA) in cold redundancy

- The radio frequency distribution assembly (RFDA) including two diplexers and five switches for signal routing to/from antennas
- Waveguides (in black) to minimize the RF path losses, while coaxial cables (in red) can be used on the transmitter side before signal amplification.

This solution is robust, as the mission is not compromised in case of failure of one transponder or TWTA.

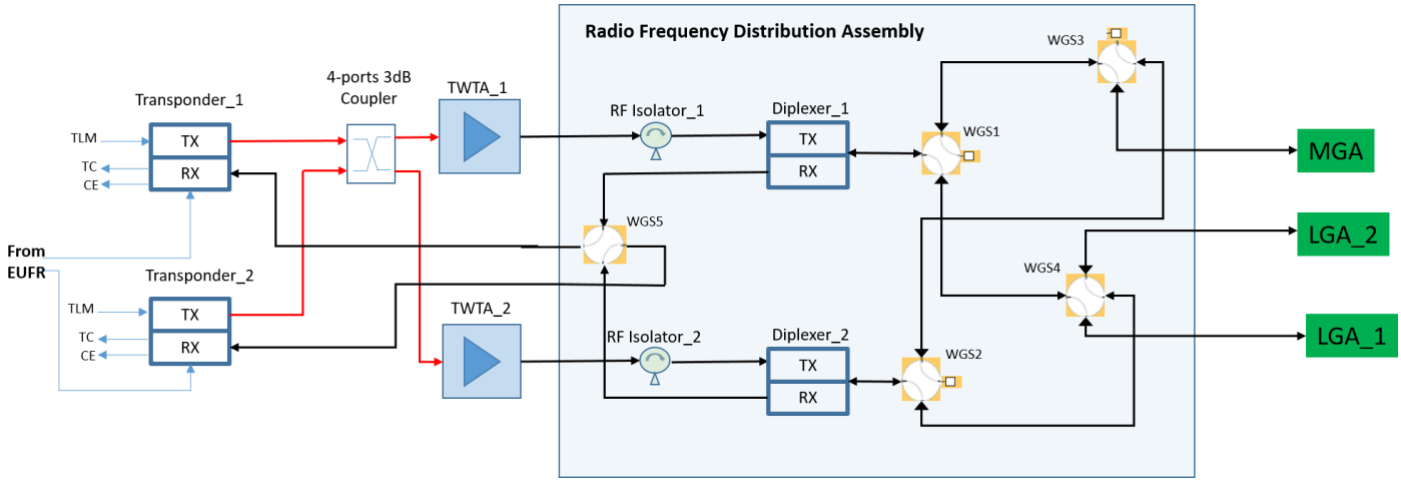

FIGURE 2 Onboard radio system architecture.

The presence of the coupler in the TX chain prior to the 10W amplification allows easy cross-strapping between the transponders and the amplifiers, improving the system reliability. Furthermore, the RFDA (cables, diplexers, ..) assembly allows for:

- (During nominal operations) keeping the nominal transponder connected to the MGA, whereas the redundant transponder (RX-ON and TX-OFF) is connected to one of the two LGA antennas and ready for TC demodulation;
- (During contingency scenarios) keeping each transponder connected to one of the two LGAs in order to assure a near-omnidirectional coverage for ground station contact;
- Minimising the RF losses and the impacts on the link budget through the use of switches instead of couplers.

The K-band TT&C transponder is a flexible unit capable of working in CCSDS PCM/PSK/PM standard modulation and in SS mode, interfacing with: a) The on-board computer for sending demodulated telecommand and receiving the telemetry data stream to be modulated and downlinked to the ground station; b) The signal generation unit (SGU), for PN code epoch time-stamping and frequency synchronization with the external ultra-stable frequency reference (EUFR), as required by the TT implementation.

Transponders also feature their own internal oscillator, typically an Oven Controlled Crystal Oscillator (OCXO), for TT&C operations when the EUFR is not required/available. Nonetheless, the synchronization of the transponder frequency with the EUFR is indispensable for the asynchronous TT function and highly recommended for SS signal frequency range acquisition that would otherwise suffer from the OCXO's frequency instability.

Technology survey and TRL. The proposed radio system architecture makes use of several enabling techniques, namely:

- The K-band instead of the more commonly used S- or X-band;
- The use of wide band signal, the current baseline consider a SS chip rate in the range of 24 Mcps;

- SS modulation based on the CDM-M scheme;
- MSPA;
- Dual mode transponder working with CCSDS standard and SS modulation;
- The interference suppression, useful in such hostile environment to avoid link interruption due to the limited rejection; of the SS codes, but in our case also to tackle the CCSDS standard signal in the contingency scenario;
- The transponder frequency flexibility.

TT&C technology is well proven and in-flight demonstrated even at higher Ka-band frequency as shown by BepiColombo (Iess et al. 2021) and JUICE (Cappuccio et al. 2020b) missions. Their transponders, built by Thales Alenia Space Italy (TAS-I), enable the novel 24 Mcps PN modulation scheme providing two-way range measurements to the centimeter-level accuracy with an integration time of only 4 s at 0.3 AU. In tracking passes with favorable weather conditions, the range-rate measurements attained an average accuracy of 0.01 mm/s at 60 s integration time. Dual-mode transponders compatible with CCSDS standards and SS modulation have already been developed for terrestrial GNSS constellations. Frequency flexibility is an additional feature, needed for LEOP operations in case of simultaneous launches. The CDM-M scheme has been proposed, studied and implemented at breadboard level for on-board application under ESA contract, both for spacecraft (Donà & Iess, 2017) and ground station equipment (ESA-GRST-STU-SOW-0010, 2016).

Algorithms for interference cancellation in SS receiver, either based on adaptive filtering (Simone et al. 2010) or on FFT solutions, have been proposed and successfully tested at breadboard level and now implemented in TT&C secure transponders. The MSPA, once supported by the CDM-M technology, is mainly a new approach for the control and operation of all the satellites of the constellation, implementing the simultaneous TT&C operation (with TC, TLM and ranging) for all the links in visibility of the ground station.

In the frame of the European System Providing Refueling, Infrastructure and Telecommunications (ESPRIT) project for the upcoming lunar space station, Gateway, TAS-I is developing the K-band transceiver (KBT) for communications and tracking, a nodal element of the Halo Lunar Communication System. The KBT is based on the IDST, a product platform under design and development by TAS-I under ESA contract. The KBT implements frequency flexibility in the range of 60 MHz at K-band and handles wide–band signal with data rate of the order of 50 Mbps.

Finally, two degrees of freedom steerable MGA represent a consolidated technology in space application, namely at X-band for BepiColombo and in dual band (X and Ka) for the JUICE missions. Off-the-shelf MGA in close alignment with ATLAS ambitions is produced by the Norwegian company Kongsberg (30 cm dish diameter, 12 kg total mass, 25 W power consumption).

Link Budget and Data Rates. The primary design feature of the proposed architecture is the MSPA concept, which concurrently enables the implementation of SBI (section 3.3). The relatively small Earth-Moon distance and the high directivity at K-band limit the size of antennas to about 26 cm. This size is however sufficient to ensure adequate data rates in the radio links. Via a pointing strategy based on the minimum enclosing circle, the pointing loss from ground can be reduced to less than 3dB for 99% of the time (and 1.3dB on average).

Table 2 reports a summary of the link budget which is computed assuming conservative conditions: for link elevation, fixed at 15°; for transmission power, limited to 200W on ground and 10W on board; for slant range, set to the maximum Earth-Moon distance; for pointing losses, set to worst-case values. In addition to that, a room-temperature Low Noise Amplifier (LNA) is considered on ground. Atmospheric attenuation, quoted from (DSN, 2015), refers to a deep space antenna site for CD=0.9. Choosing a dry site is important not only for attenuation (not negligible for K-band), but also to reduce tropospheric effects degrading the quality of radiometric observables and to guarantee and electromagnetically clean site. The latter is particularly critical for small dishes, which are prone to radiation disturbances from the surrounding environment. Transmission power from ground can be easily increased by a factor 2 or 3 (and possibly more) if enhanced uplink performances are desired. Contrarily, onboard RF power is expected to be a limited resource, as we assumed a small-sat platform dedicated to the navigation

services, in line with the Moonlight concept. Due to power and pointing requirements, a steerable MGA with a dish of 30 cm has been selected for the spacecraft.

The carrier Signal-to-Noise Ratio (SNR) for the uplink and downlink is respectively 38 dBHz and 35 dBHz, including a link margin of 3 dB (by ECSS standard). Uplink SNR is mostly limited by power-sharing loss implied by CDM-M, that is 8.5 dB for 4 (or 5) spacecraft, as reported in (Donà & Iess, 2017). Those losses become prohibitively large if the constellation is expanded in the future. The strategy, in that case, would be to form groups of 4 or 5 satellites and use additional ground antennas so to simultaneously track each group. This is a low-cost expansion given the small size of the ground terminal. The obtained signal level is considered sufficient for acquisition, provided that the onboard receiver be compatible with an acquisition window of ±130 KHz. Due to MSPA, uplink pre-steering has can only be based on a spacecraft-averaged Doppler shift and Doppler rate due to CDM-M. For downlink, each satellite can adjust its frequency independently, making pre-steering much more effective.

TABLE 1 Summary of Link Budget and Bit Rates for the ATLAS Radio Link Configuration.

	Unit	**Uplink**	**Downlink**
Frequency	**GHz**	**22.9**	**26.2**
link budget			
C/N0	**dBHz**	**49,9**	**38.5**
CDM-M losses (4 users, Gold Code)	dB	8,5	–
Link Margin	dB	3,0	3.0
S/N0 for Single Satellite	**dBHz**	**38,3**	**34,5**
Telecommands/Telemetry			
Bitrate - LDPC(128, 64) **(**required Eb/No = 4,7@ BER=1e-5)	**kbps**	**1,33**	**–**
Bitrate - LDPC(512, 256) (required Eb/No = 3,3 @ BER=1e-5)	**kbps**	**1,83**	**–**
Bitrate - CCV & R-S (r=1/2, I=5) **(**required Eb/No = 2,5@ BER=1e-6)	**kbps**	**–**	**1.00**
Bitrate – LDPC(32768, 16384) **(**required Eb/No = 1@ BER=1e-6)	**kbps**	**–**	**1.41**
Ranging			
S/N0 (Q-channel)	dBHz	26,9	31.5

Telecommand (TC), Telemetry (TM) and Ranging SNR are computed assuming the signal modulation scheme suggested in (Donà & Iess, 2017) namely Unbalanced-QPSK, with power unbalance of 1:11, for uplink, and Offset-QPSK for downlink. Ranging precision of less than 35 cm in two-way coherent mode can be obtained using a code rate of 24 Mcps, and jitter contribution from SNR of the uplink I- channel, and either the I- or Q- channel SNR for downlink. The uplink format contains only the long PN code used for ambiguity resolution and coherently generated from the shorter code used for acquisition on the I- channel. Conversely, for downlink, only the long code is used, both for acquisition and ambiguity resolution. TC and TM data-rates are reported for a couple of possible coding schemes. The target bit error rate is 10^{-5} for telecommands and 10^{-6} for telemetry. Note that the MSPA concept maximizes the data volume rather than data rate: it allows simultaneous and continuous communication with all

spacecraft. Considering roughly 22 h tracking per day, the overall downlink data volume from each satellite is larger than 110 Mbit/day.

In contingency scenarios, the small ground antenna performance is insufficient, and a dedicated larger dish of at least 13m is required. In such cases, the MSPA concept is not necessary as the link is established with a single satellite at a time, utilizing the onboard LGA and standard modulation, with residual carrier, as recommended in (CCSDS, 2021). The SS signals from a nominally operating spacecraft will be much lower in power (by about 34 dB) than the residual carrier from a 13 m ground antenna. Therefore no interferences are expected. Vice-versa, the residual carrier signal may interfere with the SS signals, in particular for the uplink, where short Gold codes are employed. This problem can be overcome using the strategies outlined above.

3 OBSERVABLE QUANTITIES FOR ORBIT DETERMINATION

A precise orbit determination is essential for the production of a high-quality navigation message, valid for a few hours without exceeding the positioning requirements of the end user. The OD process relies on the processing of radio-metric observables and on a good knowledge of the non-gravitational accelerations acting on the satellites. For a lunar constellation, the main observable quantities are range and range rate, provided by a coherent, two-way radio link as described in section 2. Although not strictly necessary to meet the SISE requirements for the satellites, SBI increases the accuracy and the consistency of the orbit determination. SBI is therefore an important enhancement of our LRNS concept.

Range Rate (Doppler). Range rate (naively interpreted as the radial velocity of the spacecraft), or Doppler, relies on the comparison between the frequency of an uplink signal generated by a highly stable frequency standard (typically a hydrogen maser) and the received signal, coherently returned by the onboard transponder. Range rate is a standard output of ground back-end receivers. State-of-the-art deep space tracking systems based on Ka-band links provide range rate accuracies in the range 0.005-0.02 mm/s at 60 s integration times, or, in terms of Allan deviation (ADEV; Barnes et al., 1971) of the frequency residuals after orbital fit, $1.7\text{-}6.8\text{x}10^{-14}$. At longer time scales (1000 s), the ADEV often reaches $5\text{x}10^{-15}$, corresponding to 0.0015 mm/s. Water vapor radiometers (WVR) and normal weather conditions are necessary to attain these values (Asmar et al., 2005, Iess, et al., 2018; Cappuccio, et al., 2020a). Doppler is the observable of choice for positioning of orbiters within the planetocentric frame, due to its extreme sensitivity to gravity gradients. For this reason, it deserves special attention in the LRNS.

The error budget of Doppler measurements for the ATLAS radio architecture has been derived from the recent data collected by BepiColombo, reported by Iess, et al. (2021) and on a previous analysis by Iess et al. (2014). We adjusted thermal noise to the SNR reported in table 1, and neglected the contribution of interplanetary plasma. Each error source in the Doppler error budget has its own spectral properties and a different relationship with the integration time. Since the numerical simulations have been carried out using Doppler data sampled at 60 s, the error budget in table 2 has been computed at 60 s integration time, scaling the values reported in the literature at a different integration time as needed. Some error sources, such as errors in the station locations and Earth orientation parameters (EOP), and mismodelling of Earth solid tides, produce larger ADEV at longer integration times. However, their contribution, which is roughly proportional to the integration time, does not affect the end-to-end noise budget even at 1000 s. The assumption of white noise at 60 s made in the simulations of the orbit determination process is therefore valid. Finally, the very small value of the ground antenna mechanical noise ($8\text{x}10^{-18}$) is a consequence of the small size of the dish. By comparison, Asmar et al. (2005) report a value of $4\text{x}10^{-15}$ @ 1000 s NASA's Deep Space Network antenna DSS 25, a 34 m dish. The value in table 2 is derived by scaling linearly from Asmar et al. (2005) and accounting for the different integration times (60 s vs. 1000 s).

Range. Range measurements are affected by random noise (thermal jitter) and systematic effects (range bias). The ranging jitter due to thermal noise depends on the available signal-to-noise ratio, both in the uplink and downlink. For a SS ranging system the jitter depends on the chip length, the pre-detection bandwidth and the loop bandwidth. With a suitable choice of parameters (pre-detection bandwidth conservatively taken as 8 times the symbol rate,

onboard and on-ground loop bandwidth of 5 and 0.1 Hz, respectively) the end-to-end range error budget ends up in a thermal jitter and range bias of 33.3 cm at 10 s sampling rate.

Although the use of an advanced WVR would improve the tropospheric calibration of the zenith wet delay to 0.5 cm (Linfield et al., 1996), in the computation of the error budget we have assumed a more conservative value of 2 cm, in line with the accuracies provided by the radiometer installed at DSA-3 (Lasagni et al., 2023) and an elevation angle of 30º. We have used also relatively large values for the station location (3 cm), since VLBI observations cannot be used with small dishes. This value is compatible with positioning via laser metrology from a fiducial point, assuming that the ATLAS antenna is located close to a large deep space tracking antenna included in the VLBI network or a GNSS station.

Differently from range rate measurements, range observables are generally affected by a significant bias, generated both by the ground and onboard electronics and antennas. Both can be calibrated with very good accuracy by means of dedicated hardware. The transponder group delay can be monitored with accuracies of < 0.1 ns by means of a calibration circuit embedded in the unit. This is the case of the BepiColombo KaT, a Ka-band transponder that is part of the MORE scientific investigation (Cappuccio et al., 2020a). The two-way group delay of the ground electronics can also be calibrated with similar accuracies, as demonstrated by Cappuccio et al. (2020a) for ESA's deep space station DSA-3 (Malargüe, Argentina).

Single-beam Interferometry (SBI). The adoption of MSPA lends itself to a straightforward implementation of single-beam interferometry (SBI). In this interferometric scheme (Bender, 1994), the phase of the two-way signal received from two spacecraft, whose directions fall within the beamwidth of a single ground antenna, are simultaneously recorded and differenced. This configuration was originally considered for a network of landers to study the interior structure of the Moon (Bender, 1994; Gregnanin, et al., 2012) and Mars (Gregnanin et al., 2014). The SBI observable retains information on the differential range between the two spacecraft, relative to the ground antenna (figure 1). Common noise sources, such as instabilities in the frequency standard and antenna deformations, are completely suppressed. If the angular separation between the two spacecraft is small (about 2º), the common noise rejection is quite effective also for propagation delays due to media (troposphere, ionosphere and interplanetary plasma). Although SBI has never been implemented or demonstrated (because of the need to uplink two coherent carriers or CDMA signals from the same deep space antenna), the generation of the SBI observables in the ATLAS architecture is expected to be straightforward. Our analysis of the SBI error budget for ATLAS shows that the differential range (phase) can be measured with a rms value of 1.3 mm (41º) for a K-band link and with the SNR shown in table 1. SBI is therefore a very precise observable quantity, which increases the consistency and the robustness of the OD.

4 TIME TRANSFER AND CLOCK SYNCHRONIZATION

As for any terrestrial GNSS, the synchronization among the clocks of the constellation is crucial to meet positioning requirements of the Moonlight LRNS, usually provided in terms of SISE. In the proposed architecture, the ground stations and the spacecraft perform ground-to-space time transfer exploiting the two-way radio link. An important difference between terrestrial GNSS and the ATLAS LRNS is the nearly complete independence between the OD process and the clock offset estimation, attained thanks to the use of two-way observables that do not involve by any means the onboard clocks. The time synchronization accuracy across the lunar constellation relies on three main factors:

- The ground-to-space time transfer accuracy
- The accuracy and stability of the satellite clocks
- The desynchronization between different ground tracking stations

The potentially detrimental effect of the desynchronization between different ground stations is largely mitigated by the MSPA approach. Indeed, a single ground station (or multiple stations of the same complex employing the same frequency standard) can simultaneously perform ground-to-space time transfer with the whole constellation, keeping the time of the constellation internally consistent. In addition, the clocks at different ground stations can

be synchronized by exchanging clock offset information immediately before and after a station handover. As we will show in the following section, accuracies in the range of 1-5 ns can be attained in the ground-to-space time transfer. If clock comparisons are carried out immediately before and immediately after the handover by the two intervening ground stations and the constellation spacecraft, also the clocks of the ground network can be internally synchronized to the same level of accuracy (1-5 ns). Binding the network time to TAI/UTC can be performed via GNSS clock synchronization. Note however that the user positioning in the lunar environment requires only a good synchronization within the constellation, which is not necessarily a synchronization to TAI/UTC. We discuss here two methods for ground-to-space time transfer and identify suitable clocks compatible with small spacecraft (mass ≈ 150-200 kg) and the required SISE.

Clock Synchronization Methods. Any measure of time desynchronization between distant clocks requires the comparison of their readings at the same coordinate time. This process involves relativistic transformations between proper time τ (the actual time read by each clock) and coordinate time t. Here we report however only a simplified formulation, where de facto proper and coordinate times are assumed to be equivalent. Indeed, relativistic transformations come into play only as deterministic corrections that need to be applied in an operational scenario. With this simplification, we only need to consider the finite speed of light.

We have identified two methods to perform ground-to-space time transfer. The first one is very similar to the well-established two-way satellite time and frequency transfer (TWSTFT) asynchronous technique (Howe et al, 1989), routinely used on Earth for comparing distant clocks and generating the UTC timescale. The second method is based on a novel approach, where the comparison is aided by ranging measurements and OD. This synchronous technique does not require the interruption of the two-way coherent link used for navigation and TT&C, therefore allowing, in principle, a much-increased frequency of the desynchronization measurements. Ultimately, both methods rely on the combination of time tags applied onboard the spacecraft and on ground.

Asynchronous Mode. The asynchronous ground-to-space time transfer relies on non-coherent links (hence the incompatibility with two-way radio-metric measurements), similarly to the terrestrial TWSTFT, where geostationary satellites are used as relays for the signals coming from/to remote terminals which are not in mutual visibility (ITU-R TF.1153-4, 2015). For the Moon the two remote terminals are in mutual visibility and the configuration is even simpler. Figure 4 shows the world lines and the scheme of the asynchronous links along with all the relevant epochs involved in the measurement. A ground clock at t_1 generates a signal transmitted from the antenna at t_2 after a delay in the TX channel mostly due to cables and electronics. The signal reaches the satellite antenna at t_3 and, after another delay in the satellite RX channel, reaches the satellite time comparator at t_4, where the onboard observable $\Delta\tau^B = t_5 - t_4$ is produced. In the downlink path an equivalent process is carried out. At t_5 the on-board EUFR generates a signal transmitted from the on-board antenna at t_6 after a delay in the spacecraft TX channel. The signal reaches the ground antenna at t_7 and, after another delay in the ground RX channel, reaches the station time comparator at t_8, where the observable quantity $\Delta\tau^A = t_1 - t_8$ sis generated.

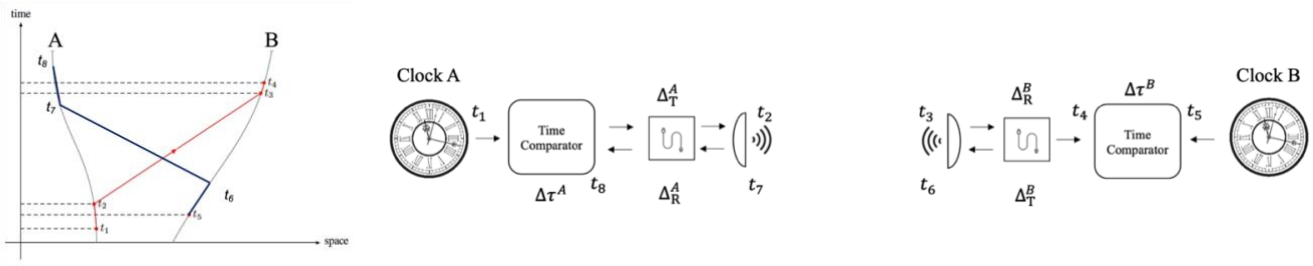

FIGURE 3 World lines and scheme for the asynchronous time transfer method. The two observable quantities, measured onboard and on ground, are $\Delta\tau^B = t_5 - t_4$ and $\Delta\tau^A = t_1 - t_8$. The other terms represent onboard and ground delays $(\Delta_T^A, \Delta_R^A, \Delta_T^B, \Delta_R^B)$ in the TX and RX path, and propagation delays (T_{23}, T_{67}).

Following the formulation given by (Duchayne et al. 2009 & Delva et al., 2012) and combining the observables from the two asynchronous links, the de-synchronization equation between the two clocks may be written as:

$$t^B(t) - t^A(t) = -\frac{1}{2}[(\Delta\tau^B - \Delta\tau^A) + (\Delta_T^A - \Delta_R^A) + (\Delta_R^B - \Delta_T^B) + (T_{23} - T_{67})], \quad (1)$$

Showing that the clock de-synchronization between ground and space clocks is the average of the two measured observables corrected for the differential delays due to electronic and propagation delays (including geometric path delays and additional effects due to Earth troposphere and ionosphere). If $t_1 \approx t_5$, the path reciprocity ensures most errors cancel out in the differentiation procedure, including errors in OD. The measurement uncertainty could be as low as ~ 0.3 ns, in line with the uncertainty reported in the BIPM Circular T (June 9th, 2023).

A drawback of the asynchronous method is the need to switch the operational mode of the onboard transponder from coherent to non-coherent, therefore interrupting the acquisition of radio-metric data at the ground station. The number of clock comparisons performed during a tracking pass is therefore limited. Although its practical realization requires some changes in the hardware of state-of-the-art deep space transponders, the current digital architectures make such modifications easy to implement.

Synchronous Mode. In any two-way coherent radio-metric measurement (range or Doppler), the mathematical model of the light-time considers the time of three participating events (neglecting, for now, the internal spacecraft delays):

- t_1: epoch of signal transmission from ground
- t_2: epoch of signal reception onboard the satellite
- t_3: epoch of signal reception on ground

Two-way ranging observables represent a measure of the round-trip-light-time (RTLT $= t_3 - t_1$), that multiplied by the speed of light c provides a measure of the distance travelled by the signal in the uplink and downlink paths. The ground clock directly measures t_3, while t_1 and t_2 are retrieved by solving backward for the light-time solution (Moyer, 2003), a mathematical pillar of any orbit determination code. Instead, the onboard clock has direct access to t_2, measured in terms of its proper time and converted to coordinate time. In the two-way coherent configuration, the ground-to-space clock desynchronization may be therefore written as:

$$\text{Desynch}(t) = \hat{t}_2(t) - t_2(t) = \left(t_3(t) - \frac{\rho_{23}(t)}{c}\right) - t_2(t), \quad (2)$$

Where $\hat{t}_2(t)$ is the onboard time retrieved by the orbit determination solution through ρ_{23}/c, the one-way return light-time. $t_2(t)$ are the readings of the onboard clock. This difference represents the desynchronization between ground and space clocks. The onboard time-stamping operations are triggered by a 'Code Epoch' (CE) signal, activated by a specific chip of the spread spectrum signal. The proposed Truncated Maximum Length (TML) sequence for the uplink spread spectrum code has a length of $256 \cdot (2^{10}-1) = 261888$ chips. Assuming a chip rate of ~ 24 Mcps, the chip length $\tau \approx 41.6$ ns and the code repetition period is $T_{TML} \sim 10.9$ ms.

Two aspects must be carefully considered when this method is used: the capability to solve for the code ambiguity and the precise association of the CE arrival to the time-stamping operation carried out by the clock assembly. Data encoding and transmission through the telemetry channel may indeed add a certain delay Δ_2, that, depending on the adopted coding method, may even cause Δ_2 to exceed T_{TML}. However, this delay is largely deterministic and could be easily calibrated in post-processing. Therefore, what really matters is that the residual uncertainty $\delta\Delta_2 \ll T_{TML}$, a condition that can be easily met. When the signal is received on ground, a similar time-tagging operation is triggered by the received CE signal and the epoch t_3, provides $\hat{t}_2$ through the OD process. In parallel, telemetry data about t_2 is downloaded by the satellite. This may add an additional delay Δ_3 for which same considerations as for Δ_2 apply. Figure 5 shows the scheme for the two-way coherent time transfer method.

The performances of this time synchronization method depend on: a) the precision of time-stamping operations (σ_{t_2} and σ_{t_3}) and b) the orbit determination accuracy in the line-of-sight direction (σ_ρ). The LOLA laser altimeter of the Lunar Reconnaissance Orbiter has achieved a time-stamping precision of about 0.5 ns (Bauer et al. 2017), while numerical simulations (see section 5) show an OD accuracy along the line-of-sight better than 10 cm, corresponding to 0.3 ns. We may therefore conservatively assume an overall contribution of the ground-to-space time transfer procedure at 1 ns level to the time synchronization across the entire lunar constellation.

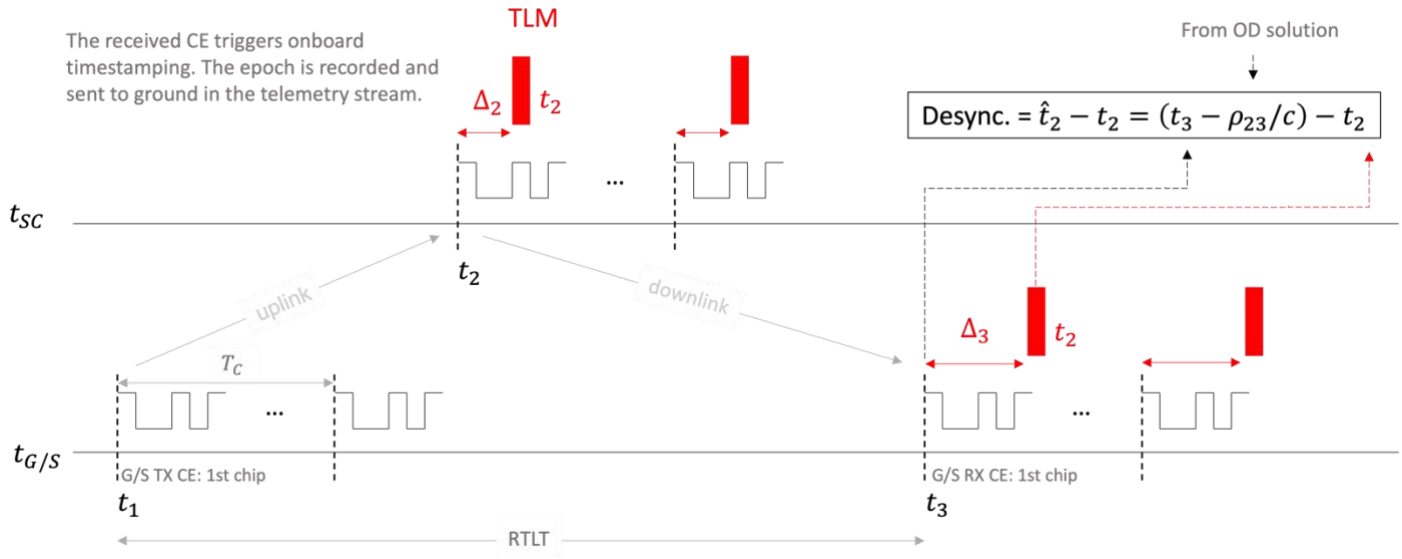

FIGURE 4 Scheme for time synchronization with the two-way coherent approach. The delays Δ_2 and Δ_3 introduced by data encoding/decoding in the telemetry (TLM) transmission may even exceed the code repetition period. The associated uncertainties $\delta\Delta_2$ and $\delta\Delta_3$ must be $\ll T_L$.

Onboard Clocks. The selection of the onboard clocks is a trade-off between performances (accuracy and stability), SWaP-C (Size, Weight, Power & Cost) and technology readiness level. Although the MSPA approach allows for nearly continuous contact between each satellite and the tracking stations, the system shall be able to work also when contact with Earth is interrupted for a few hours. This requirement rules out the use of Microchip Scale Atomic Clock (CSAC), whose drift would lead to SISE >100 m in a few hours. Deep Space Atomic Clock (DSAC)

Table 2 SWaP and performance comparison (ADEV) among different space clock technologies (data sheets available at the companies' web sites). The ADEV at different timescales is the maximum value for each technology.

	RAFS (Orolia – Rb Galileo)	**USO (AccuBeat)**	**miniRAFS (Orolia)**
Size (mm x mm x mm)	217x124x117 (2.4 liters)	167x107x131 (2.34 liters)	107.5x67.5x53.5 (0.39 liters)
Mass (kg)	3.3	2.0	0.45
Power (W)	< 30	< 5	< 10
ADEV(1s)	5e-12	2e-13	1e-11
ADEV(10s)	2e-12	2e-13	3e-12
ADEV(100s)	5e-13	2e-13	1e-12
ADEV(1000s)	2e-13	2e-13	3e-13
ADEV(10000s)	5e-14 (drift removed)	1.4e-12 (6e-13 if drift removed)	1e-13 (drift removed)

and Galileo Passive Hydrogen Maser (PHM) clocks are the best choices in terms of absolute performances (especially for their long-term stability, $<10^{-14}$ at 1-day timescale) but at the cost of a mass not lower than about 10 kg. Galileo Rb clock long-term stability is about 10 times worse, but the error contribution after 1 day is still

acceptable (~ 1 m) and the mass is compatible with a small/minisat (3.3 kg). Two other attractive solutions are miniRAFS and USOs, given their low mass and power consumption. Although USO generally suffer from large drift, the Accubeat USO, developed for ESA's JUICE mission, combines an excellent short-term ADEV with good performances at longer time scales (~ 10^{-12} at 10000 s). The table below summarizes a SWaP and performance comparison among RAFS (Orolia), USO (from AccuBeat) and miniRAFS (Orolia). A rough estimation of the clock error contribution to the positioning error at different time scales may be estimated as $\Delta p \approx c\tau\sigma_y$.

5 ORBIT DETERMINATION AND SATELLITE EPHEMERIDES

The lunar constellation considered in our concept is made up of four satellites in Elliptical Lunar Frozen Orbits (ELFO). The Keplerian elements of the ELFO orbits have been selected to minimize orbit-keeping maneuvers while providing a good coverage of the southern polar regions of the Moon, the main target of future lunar exploration missions. The selected combination of semimajor axis, eccentricity, and inclination nearly zeroes out the change in eccentricity and argument of pericenter due to third body and non-spherical gravity perturbations. The satellites are distributed in two orbital planes of inclination 61.96º and 54.33º, and the right ascension of the ascending node equal to 59.27º and 277.53º, respectively. The orbits have a common eccentricity and semimajor axis (0.6383 and 9750.73 km), and a period of 24 h. The maximum distance between any pair of satellites is below 20000 km, an important quantity for the selection of the size of the ground antennas. The pericenter altitude is 14237.22 km, suitable for a prolonged coverage of the southern polar region.

The ground tracking coverage of the lunar constellation mostly depends on the location of the tracking sites on Earth. Deploying the Moonlight antennas at the sites of ESA/ESTRACK deep space tracking stations would leverage the existing infrastructure, most notably hydrogen maser frequency standards and WVR for wet tropospheric calibrations (currently available only at the Malargüe site). For our test cases we have thus considered tracking from New Norcia (Australia), Cebreros (Spain), and Malargüe, Argentina. However, the longitude coverage from these sites is not optimal due to the large gap between Malargüe and New Norcia. In order to ensure continuous coverage, we have considered also a case where a fourth tracking station is located at Mauna Kea, Hawaii (USA). With this configuration tracking interruptions occur only during lunar occultations, which may last up to ~ 1 hour.

Dynamical Model. The numerical simulations are split in two main steps: the simulation phase, aimed at generating the reference trajectories and the associated, synthetic, observed observables, and the orbit determination process, performed using a batch estimation filter. The goal of the second step is to retrieve the reference orbits using the observed observables (with coloured or white noise added).

The dynamical model of the spacecraft in the simulation step accounts for the gravitational monopole accelerations due to the Earth, the Moon, and Solar System's planets, in a relativistic 1-PN formulation; The spherical harmonics coefficients of the Moon, up to degree and order 20; The spherical harmonics coefficients of the Earth, up to degree 2; The non-gravitational acceleration due to the solar radiation pressure (SRP). Other sources of non-gravitational accelerations, such as those due to the lunar albedo and the spacecraft anisotropic thermal emission, have not been included in the model due to their small magnitude.

The spacecraft is represented as two plates and a sphere. The first plate models solar arrays (area of 11 m^2), pointed toward the Sun, while the second plate models an antenna dish (0.40 m^2 area) constantly pointed toward the Earth. The spacecraft bus is modelled as a 1m radius sphere. The mass of each spacecraft has been set to 230 kg, thus producing an area-over-mass ratio of ~0.061 m^2/kg, corresponding to a solar radiation pressure acceleration of about $3x10^{-7}$ m/s^2. This area-to-mass ratio, approximately 3 times larger than for the Galileo satellites, may lead to pessimistic results. However, lacking information on the satellite design, this conservative assumption provides adequate margins, especially for ephemeris aging.

In the estimation step, we introduce an error in the antenna plate's area (area of 0.40 m^2), thus a mismodelling in the solar radiation pressure acceleration, to emulate the inaccuracies of the dynamical model that characterize a realistic orbit determination process. To compensate for the error in the SRP, we have introduced empirical

piecewise-constant accelerations into the spacecraft dynamics, namely a constant acceleration vector with components on each axis of the ICRF frame. The associated empirical acceleration parameters are updated every 4 hours, their nominal value is set to zero and they are assumed to be uncorrelated among difference batch interval, while their a priori uncertainty is of the same order of magnitude of the SRP mismodelling (7.5×10^{-9} m/s^2).

Test Cases. For the full concept validation, several simulations have been carried out, considering different scenarios (X- as well K-band, SBI observables included or not in the OD filter, 3 or 4 tracking sites). In each of these cases, a Monte Carlo-like analysis has been performed by changing the epoch of the initial conditions of the constellation to have full coverage of the Earth-Moon relative geometry over 28 days (thus covering a full lunar sidereal month). 577 arcs have been simulated, by shifting forward the initial conditions at steps of one hour. Each data arc is 4 days long. To analyze the ephemerides ageing, we integrated the trajectory for an additional day, propagating forward the state and the covariance matrix from the last data point in order to assess the degradation of the state error and uncertainty with time, when no observations are available.

Considering that a large number of cases has been simulated in the the Monte Carlo analysis, before presenting the cumulative results, we report on positioning performances of the constellation for a representative data arc in order to understand the characteristic trends of the error and uncertainty over time. We present the results for the baseline configuration, thus considering:

- K-band and MSPA;
- Doppler, range and SBI observables;
- Ionospheric media calibration with GNSS (10% uncalibrated) and tropospheric media calibration with AWVR (5% uncalibrated);
- Three tracking sites (putatively located close to ESA/ESTRACK ground stations).

For the initial state vector of each satellite, a randomly chosen bias with a standard deviation of 1 m for each position component and 0.1 mm/s for each velocity component has been assumed, to account for realistic errors in the initial state. For the a priori uncertainty we have used much larger values (1 km and 1 km/s) that basically corresponds to having an unconstrained a priori solution.

We analysed the orbital accuracies for different reference frames, namely the ICRF (Moon-centred), RTN (to Moon) and RTN (to Earth), for the different spacecraft of the constellation. The radial-transverse-normal (RTN) toward the Earth (or Moon) is defined with the R-axis pointing from the Earth (or Moon) toward the spacecraft, the N-axis is along the orbit normal (parallel to $r \times v$), and the T-axis completes the right-handed frame. The accuracies are comparable for the 3 directions in the first 2 reference frames, while in the last one, the radial direction is extremely more accurate than the other two (< 10 cm). This is related to the fact that, in this frame, the radial component is approximately equal to the line-of-sight (LOS, i.e., Earth-satellite vector) and the observables are collected along this direction. The positioning accuracy in the direction of the line-of-sight (LOS) is especially important to evaluate the performance of time transfer.

Figure 5 reports the RSS of state determination accuracies (position and velocity) for the four satellites in the chosen arc. The three spacecraft have comparable state vector uncertainties, given that the tracking schedule is very similar for all nodes. The periodic, rapid decrease in both the uncertainty and the error is related to the pericenter passes where the OD is more accurate since the orbital dynamics is strongly bounding the spacecraft to the gravity field of the Moon, given that the satellite is closer to it. Figure 5 shows a vertical solid black line that represents the epoch of the last acquired data. The position uncertainty and error after that time result from a pure propagation of the state vector (no measurements). The reported uncertainties and errors after the acquisition of the last data point represent a characteristic case of ephemerides aging.

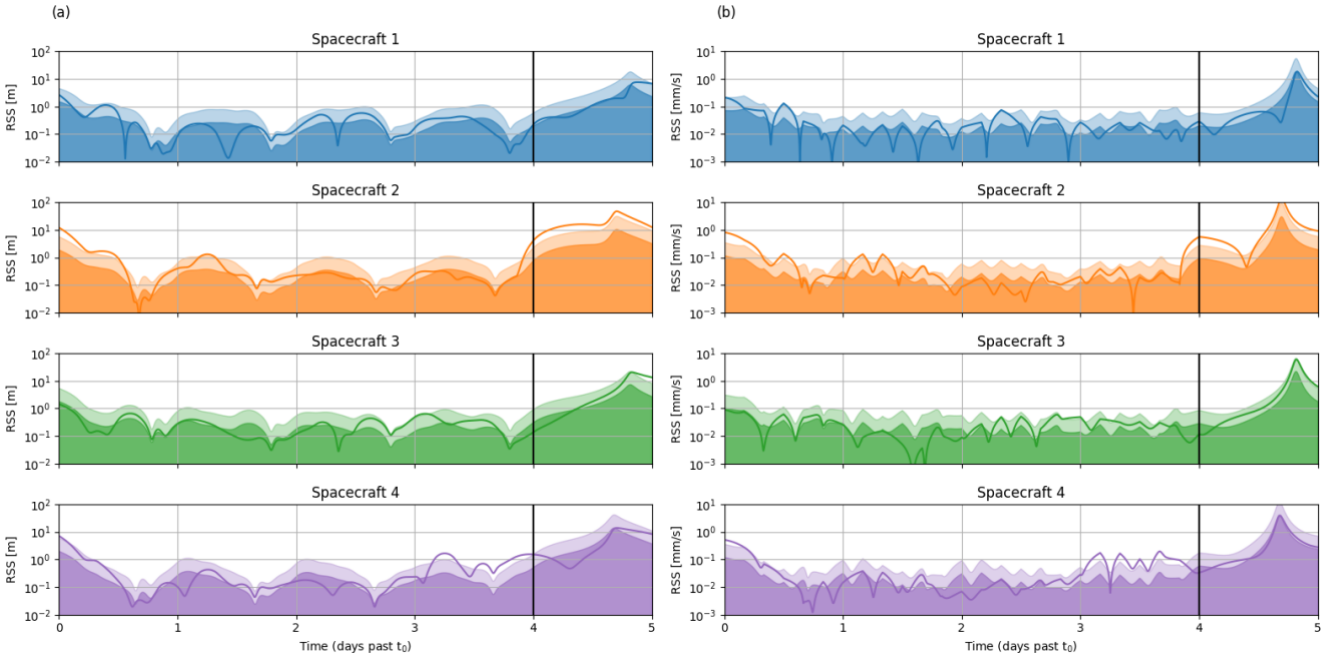

FIGURE 5 RSS of position and velocity uncertainties (shaded areas, 1-σ and 3-σ) and errors (solid lines) for the four spacecraft.

Ephemeris Ageing. In order to assess the performance of the proposed LRNS architecture, we evaluate the ephemerides ageing, and to do so, it is necessary to numerically propagate forward for some time (we selected 1 day) the estimated covariance and error of the state of the four satellites. The ephemerides ageing represents one of the main contributions to the overall SISE, defined as the sum of position and clock errors

$$SISE = \sqrt{(x-\bar{x})^2 + (y-\bar{y})^2 + (z-\bar{z})^2 + c^2(t-\bar{t})^2} \ , \tag{8}$$

Where x, y and z are the true coordinates of the spacecraft at time t and $\bar{x}, \bar{y}, \bar{z}, \bar{t}$ are the broadcasted coordinates and time ($\bar{t}$ includes the clock corrections). Apart from relativistic transformations, SISE is independent of the chosen reference frame and time scale. The two main elements that affect the ephemerides ageing process are the error at the last data point, so at the start of the ageing and the accuracy of the spacecraft dynamical model. Since an accurate knowledge of the dynamics is crucial for propagating forward the spacecraft state, its mismodelling plays a crucial role.

Figure 6 shows the distribution of the error at the last data point for each arc and for each spacecraft of the constellation as a function of the corresponding spacecraft true anomaly at the last data epoch. The lower density of points near the pericenter is related to the shorter time spent by the spacecraft near zero true anomaly. This data representation highlights how the positional accuracy at the last data point decreases significantly if the spacecraft is close to the orbit apocenter, with large variations. Indeed, given the weaker gravity gradient at the apocenter, Doppler data provide less information, therefore leading to increased state covariances.

The Monte Carlo simulations provide an insight on the trajectory error as a function of the time past the last acquired data for all the analysed cases. Adding this contribution to the clock synchronization error provides the SISE (defined in the previous section). Figure 7 shows the evolution of the SISE when considering the clock contribution from miniRAFS. The different curves represent the mean value of the error, and the value for which 95% and 99% of all cases are below a certain error, taking into account also different clock realizations. Not surprisingly given the relatively good long-term stability of miniRAFS, the SISE is largely dominated by orbital errors, as shown in figure 9. (This finding is true also for RAFS and, to a lesser extent, USO.)

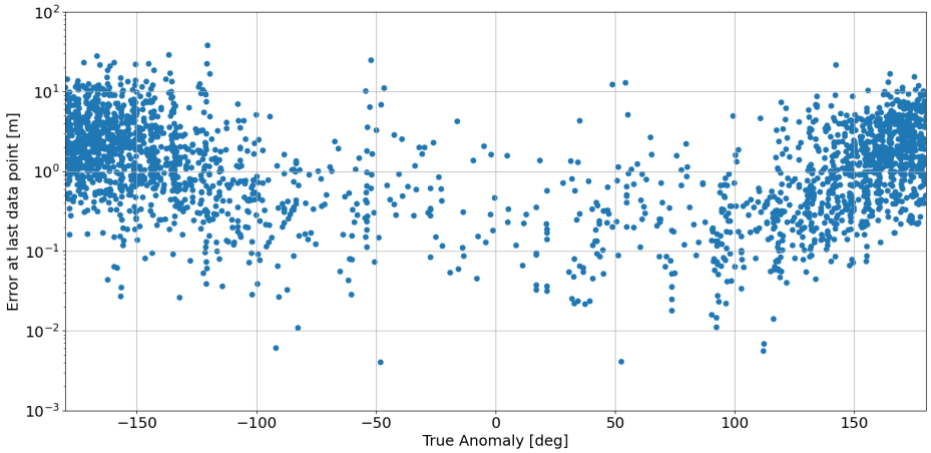

FIGURE 6 Distribution of the error in the last data point acquired in each arc as a function of the corresponding satellite true anomaly.

The space components of the SISE are affected not only by the orbit determination accuracies, but also from the orbit representation error in the navigation message. We have found that if each navigation message refers to an orbital span of one hour, using an approximation with Chebyshev polynomials of degree 10 (11 coefficients), the 95-percentile of the orbital fit error is smaller than 11 cm. This contribution to the SISE is an order of magnitude smaller than the orbit estimation errors and therefore it was neglected.

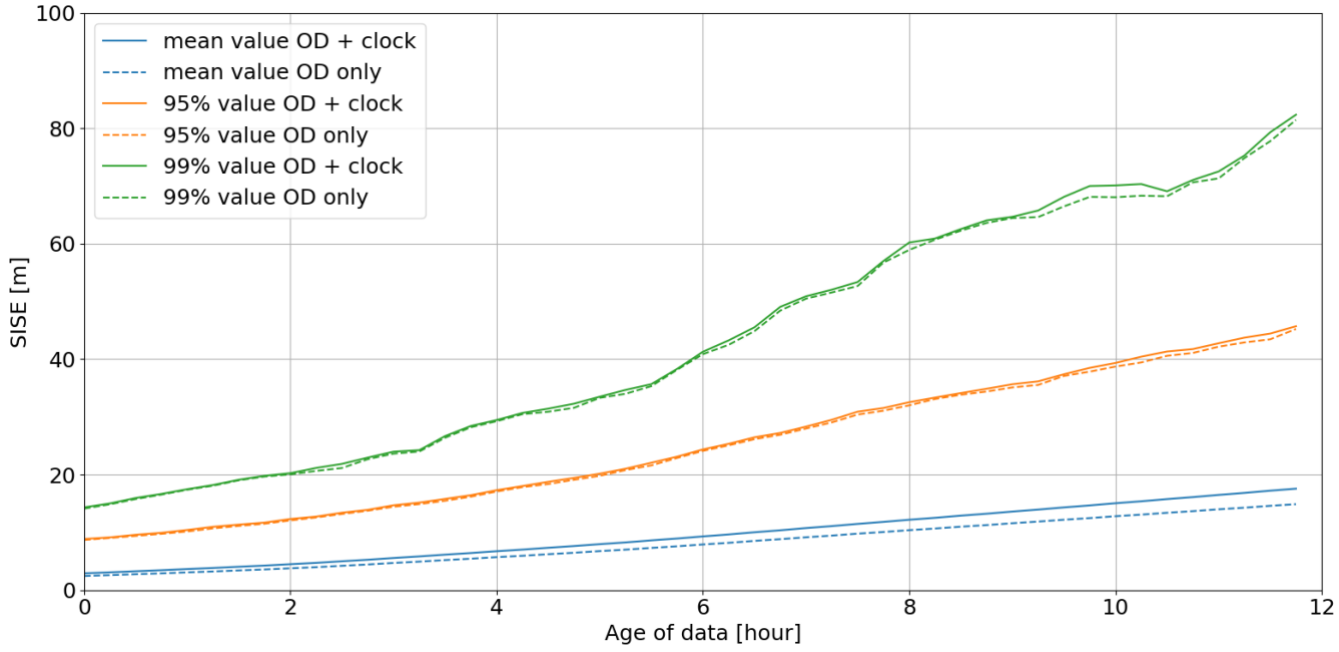

FIGURE 7 Evolution of SISE with time as a function of the aging time for miniRAFS. Solid lines: SISE due to both OD and clock errors; Dashed lines: OD contribution to SISE; Blue curves: mean value; Orange curves: 95% percentile; Green curves: 99% percentile (for all simulated arcs and clock error realizations).

The attainable OD performances of the proposed MSPA architecture depend on several design choices that ultimately affect the type, quantity, and accuracy of the observables. Table 9 reports a comparison of the attainable ODTS accuracies for different cases, entailing the use of X or K band, a different combination of observables (e.g., no SBI) and the use of a fourth, additional tracking station (putatively located in Mauna Kea, Hawaii) to ensure continuous tracking and visibility. These different cases are informative on the main design choices of a LRNS.

TABLE 3 SISE performances under different operational scenarios.

SISE cases with miniRAFS	**SISE error @ 12 h**	**Ephemeris aging (time to reach 25 m)**	
	Mean value	95% value	99% value
Doppler & range & SBI (K band)	17.57 m	6 h 10 min	3 h 20 min
Doppler & range (K band)	18.41 m	6 h 03 min	3 h 21 min
Doppler & range (X band)	24.12 m	4 h 29 min	2 h 21 min
Doppler & range & SBI (K band) with an additional tracking site	14.01 m	8 h 50 min	5 h 01 min
Doppler & range & SBI (X band)	21.77 m	5 h 22 min	2 h 43 min

The simulations confirm that a system based on K-band radio links outperforms the X-band counterparts. The limited bandwidth available for X-band SS modulations (recommended at 6 MHz by the Space Frequency Coordination Group - REC SFCG 41-1) significantly degrades the accuracy of range measurements (reduced to 130 cm compared to 33 cm at K-band). Moreover, the lower frequency amplifies the bias and noise introduced by the ionosphere in both Doppler and range measurements by a factor of 10. Although the benefits of SBI may appear limited, the inclusion of a third data type alongside Doppler and range measurements enhances the overall solution's robustness as it allows for easier identification of inconsistencies. We found also that the utilization of SBI significantly enhances the performance of an X-band radio system by effectively mitigating ionospheric effects through common mode rejection. As a final remark, the continuous coverage provided by a fourth station, coupled with K-band observables, yields the highest accuracy in orbit determination and minimizes ephemeris aging.

6 REFERENCE FRAMES AND TIME SCALES

These topics have been addressed in CD-1-Annex-B. The definition of a lunar body-fixed coordinate system and frame is essential to locate a point on its surface and to establish accurate cartography. Two body-fixed lunar reference systems have been used in the past, namely “Mean Earth” (ME) and “Principal Axes” (PA). The coordinates of a point on the lunar surface may differ up to 500 m. Although the final choice among these two systems is deferred to the NASA-ESA coordination group and, ultimately, to the IAU, we proposed two reference systems, an inertial one, the Moon-centred inertial lunar reference system (LCRS), and a body fixed one, the lunar body-fixed reference system (LRS).

Based on the concept of the geocentric celestial reference system (GCRS) as given in the IAU 2000 Resolution B1.3, we propose to define an inertial frame, the LCRS, centred at the Moon center of mass, associated with a metric tensor based on (Damour et al., 1991) but adapted to the gravitational environment of the Moon. A lunar time scale is also defined associated with this metric tensor. This system shall be used for navigation and the integration of the equations of motion in the vicinity of the Moon.

We outlined the definition of a lunar time scale associated to the LCRS. The UTC time scale is used for the recording of the observations from the ground. For the definition of the selenodetic frames or when one uses the Earth-based observations for studying the dynamics of the moon, the UTC time scale is transformed into TDB. The GPS or Galileo time can be used as intermediate time scales between lunar orbiters and ground-based stations as it is proposed in the case of receivers of Earth GNSS signals in lunar orbit. For the Moon surface datation or for the constellation orbiting the Moon, we define TCL (Lunar-centric coordinate time), the relativistic time scale at the center of mass of the Moon, similar to TCG, the relativistic time scale at the geocenter. Using the intervening metric tensors, we computed the relation between TCL and TCB, that can be used to define TCL as related to TCB, and then TCL to TCG.

Similarly, using the intervening metric tensors, we presented the transformations between coordinates in BCRS and LCRS.

The realization of the LCRS can be done using different lunar and planetary ephemerides. We consider two generations of ephemerides, DE421 which is the present reference for the definition of lunar ME frame, and INPOP19a. These two ephemerides differ as DE421 model does not account for the core-mantle interactions and the shape of the fluid core. More than 11 years of additional observations were also included in the INPOP19a construction. Figure 8 shows the differences in term of localization of the Moon relative to the Earth using DE421 and INPOP19a over 5 years. The maximum differences of about 1.5 meters are obtained in the z-direction. The ratio between the gravitational mass of the Earth- Moon barycentre obtained with DE421 and with INPOP19a differ from unity by $(1.2 \pm 10^{-11}) \times 10^{-8}$.

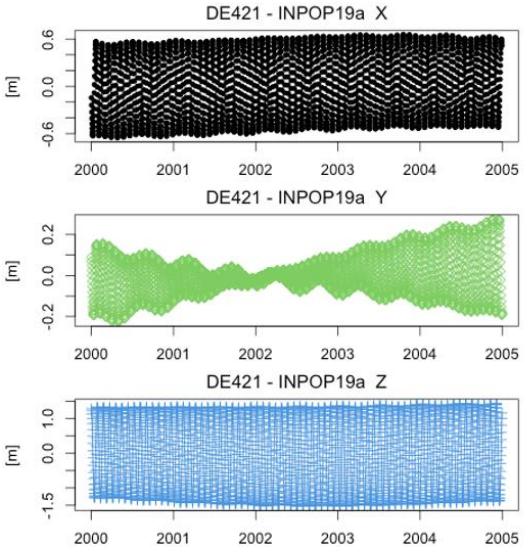

FIGURE 8 Differences in meters on the Moon center positions relative to the Earth estimated with DE421 and INPOP19a in the ICRS.

In parallel to the LCRS, it is requested to define a frame fixed to the Moon, as the ITRS has been defined as an Earth-fixed frame. This frame, called LRS, will be defined based on the PA properties, hence on the measurement of the quadrupole tensor of the lunar gravitational field. The realization of such a system could be obtained by using planetary and lunar ephemerides. We considered different accuracy assessments for the LRS realisations, starting with the differences between the PA realisations using different planetary and lunar ephemerides. We then considered the propagation of the PA covariance matrices with time. We then discuss the link accuracy with other methods such as altimetry and images obtained from LRO. Finally, we discussed alternative time scales that can be more appropriate than the TCL for the user localization or spacecraft.

7 PROXIMITY LINK

The study addressed also the radio frequency signal modulations for lunar navigation services (Task 3 in the SOW), with the aim at identifying the most appropriate radio frequency signals to support the LRNS. Both one-way service and two-way service towards the end user were considered.

One-way Service. For the proximity link in one-way mode, the following topics have been addressed in CD-2:

1) One-way service signal modulation schemes (including also a review of the standard modulation schemes adopted by current Earth GNSS;
2) The reference modulation schemes selected for the analysis, including modulation of the pilot channel and a comparison of the ACF shapes
3) The performance metrics adopted for the analysis, including the acquisition stage, the tracking stage, the effects of multipath, and susceptibility to possible radio frequency interferences.

4) A comparative performance analysis of the different schemes, using the metric indicators mentioned in point 3), and including an assessment of multipath and intrasystem interferences and protection.
5) Preliminary LRNS one-way service signal proposal .
6) An assessment of the RF compatibility with WiFi.

The analysis carried out indicated that the different pilot channel modulations (BOC(5,1), BOC(5,2), BPSK(4) and BPSK(5) have been considered) have contrasting benefits/drawbacks.

While BPSK(1) is suggested for the data channel, three main options seem the most suitable for the pilot component:

- BOC(5,1) outperforms the other choice from a number of points of view. Its main drawback stays in its sensitivity to interference. If such a solution will be selected, a proper protection of the RF spectrum close to its subcarriers must be guaranteed. Additionally, proper techniques for detection and mitigation of interference should be adopted in reception
- BPSK(5) seems a promising alternative. Even though the tracking performance are worse than BOC schemes, it is less susceptible to multipath and interference.
- BPSK(4) can be an alternative to BPSK(5), as having similar performance, allows more power collected by a 16 MHz receiver front-end.

The performance of these three modulations are very close. As a further and more general consideration, we point out that one of the motivations that brought to the advent of BOC modulations was assuring the interoperability among different GNSS signals in the L band (e.g., Galileo E1 and the heritage GPS signal). However, at this stage, no other navigation signals are expected in the considered band for the LRNS.

In the framework under consideration, the main motivations for choosing BOC(5,1) instead of BPSK(4)/(5) are: better tracking performance and higher isolation from the BPSK(1) data channel. However, BOC(5,1) entails a number of issues, namely multi-peaked ACF, increasing the probability of side-peak tracking, higher sensitivity to multipath, and lower robustness against interferences, with potential issues due to the vicinity of the lower sub-carrier to the WiFi band. Overall, considering that BPSK(4) and BPSK(5) can achieve performance quite close to BOC(5,1) but they can be more robust against potential interfering sources (with specific regard to the WiFi band), they are preferred.

A preliminary proposal for the one-way signal structure is provided in table 4. This considers a data+pilot signal with 50/50 power sharing (even though 25/75 could be successively reconsidered), while BPSK(4) and BPSK(5) have been selected for the pilot channel.

TABLE 4 Preliminary LRNS one-way service signal proposals

Frequency band	[2483.5 – 2500] MHz	
Carrier frequency	2492.028 MHz	
Access technique	CDMA	
Signal component	Data (I)	Pilot (Q)
Power sharing	50 (25)	50 (75)
Modulation scheme	BPSK(1)	BPSK(4)/BPSK(5)
Primary PRN Code duration	1 ms	1 ms

In addition, CD-2 reports on the analysis of the navigation message coding schemes and performance comparison. The following topics have been addressed:

1) Channel coding, including CCSDS recommended schemes, coding schemes used in GPS and Galileo, convolutional codes, low-density-parity-check (LDPC) codes.

2) Performance analysis and comparison, including performance of LDPC and convolutional codes in AWGN, performance of LDPC and convolutional codes in fading channels, decoding complexity, comparison of performances of GPS L1C versus Galileo E1 OS.

A final comparison in terms of advantages/drawbacks of convolutional and LDPC codes is shown in table 5. Additionally, the following recommendations can be derived from the GPS L1C versus Galileo E1OS performance comparison/analysis:

- Limit data content to navigation data or at least clearly separate navigation data from additional service to guarantee timeliness
- Data transmission rate should be kept as low as possible since it heavily impacts the robustness (trade off robustness/timeliness)
- Block duration of some seconds are a good compromise between latency and robustness to fading
- Use efficient error protection techniques.

On the basis of the above results, it can be concluded that LDPC represents quite a promising option and could be adopted as a viable choice.

TABLE 5 Comparison of convolutional codes versus LDPC

Aspect	Advantages	Drawbacks
Convolutional codes	▪ Largely used in GNSS (i.e., both GPS and Galileo) ▪ They permit continuous decoding via the Viterbi algorithm or sequential decoding	▪ For a fixed code rate (e.g. 1/2) they experience a loss in power efficiency with respect to LDPC in the AWGN channel ▪ Less robust than LDPC codes in presence of burst of errors
LDPC codes	▪ They outperform convolutional codes in both power efficiency and spectral efficiency ▪ Robustness in presence of burst of errors ▪ Different code rates recommended by CCSDS to trade off spectral and power efficiency ▪ Iterative decoding could allow ✓ to use a fixed number of iterations for fixed latency of blocks with the same code rate and block length. ✓ to configure the amount of LDPC decoding iterations for trading-off throughput and error correction performance	▪ Less used in GNSS (i.e., GPC L1C and Beidou) ▪ Penalty due to finite block size increases with decreasing block length ▪ Decoding done via an iterative procedure: performance depending on the specific implementation and on the number of iterations

Two-way mode. For the proximity link in two-way mode, the service signal modulation schemes have been analyzed, taking into account the CCSDS recommended coding schemes. We presented some considerations on the spectrum regulations and recommendations, then we analyzed the data transmission and PN ranging based on Tausworthe codes, their spectral properties, acquisition performance, and ranging system accuracy, Finally, we presented an analysis for data transmission and PN ranging based on DSSS, and a summary of the LunaNet draft proposal.

Advantages related of the proposed Tausworthe codes for ranging are:

- The possibility to maximize the re-use of existing methods already explored in the context of ground to space ranging;
- The flexibility allowed by the two T4B and T2B codes, basically obtained from the same probing sequences and with the same logic by simply changing the vote given to the clock component, that allows to put first the requirement for the acquisition time or the requirement on ranging accuracy depending on the specific conditions.

Potential disadvantages are:

- The possibility of mutual interference between telecommand and ranging, and between telemetry and ranging when the signals are transmitted simultaneously on the same carrier;
- These PN codes are not intended for CDMA applications or for power flux density reductions, particularly because of the strong spectral component at the range clock frequency: this implies the need for different strategies (e.g. time division) if a multiple access is required.

Potential solutions allowing CDMA are rely on direct sequence spread spectrum (DSSS). This alternative (or complementary) approach allowing CDMA can be derived from the recommended standards specifying a set of CDMA DSSS modulation schemes for CCSDS users. (Note: these schemes are intended for use in space-to-space communications links.)

DSSS provides the following functions over a space link:

- Multiple simultaneous users;
- Reduction of the signal PSD and minimization of Multiple Access Interference (MAI);
- Reduction in interference susceptibility (including jamming and multipath);
- Capability of supporting PN ranging and time transfer operations.

Advantages related to the choice of this approach for ranging are:

- PN codes are intended for CDMA applications thus allowing simultaneous use by multiple users;
- The PSD of a spread signal is greatly reduced compared to that of an unspread signal, by a factor of the PN rate to the symbol rate: this implies a reduced interference on systems operating in the same or close bandwidths;
- The possibility to capitalize on existing methods, hardware and concepts, coming from the Earth GNSS scenario considering the high similarity of the single link with the one-way involved by GNSS and possible synergic approaches between one-way and two-way.

Potential disadvantages are:

- The incomplete orthogonality of the signalling format implies that cross-correlations are present, thus inducing MAI noise, hence performance may degrade with the increase in the number of users;
- Higher complexity.

8 REPRESENTATION OF THE NAVIGATION MESSAGE

An accurate positioning using the navigation satellites relies on orbit (ephemeris) and clock information generated by the control center, uploaded to the spacecraft and broadcasted to the end user. While the clock offset representation is straightforward (a degree-2 polynomial would suffice), several possibilities exist for the ephemeris representation. We considered three ephemeris representation methods:

- Keplerian parameters with corrections accounting for orbit perturbations (Galileo-like orbit representation)
- Chebyshev polynomials (similar to the representation of the lunar and planetary ephemeris used for the reference frame transformations)
- Cartesian position series (GLONASS-like orbit representation).

The Cartesian positions (or positions & velocities or positions & velocities & accelerations) require the procedure of orbit numerical integration on the user side. The numerical integration provides high-accuracy results; however, a user must have a full set of models accounting for orbit perturbations, which includes the lunar gravity field, solar radiation pressure, Earth, Sun, and planetary orbit perturbations, albedo, relativistic effects, time-variable gravity field due to tidal effects, etc. The Cartesian representation limits the possible applications for real-time solutions

unless the simplified model of orbit perturbations is used due to the computational complexity on the user side. Therefore, we do not recommend the Cartesian representation for the lunar orbiter.

Chebyshev polynomials have a simple representation and implementation. The accuracy is directly related to the number of coefficients, i.e., the order of the polynomial expansion; however, even the millimeter accuracy is possible. A similar representation based on Chebyshev polynomials will be provided for the reference frame transformation between Selenocentric Celestial Reference Frame (for orbit position representation) and Lunar-fixed Reference Frame (co-rotating with the Moon for the representation of the receiver positions).

The Keplerian parameters with corrections accounting for orbit perturbations are used in the GNSS systems, such as Galileo and GPS. However, the standard representation was designed for circular orbits of high-orbiting satellites, for which the gravity field perturbations of Keplerian parameters can be simplified to the main terms causing secular drifts or once/twice-per-revolution perturbations of Keplerian elements. However, for spacecraft in the ELFO orbits considered in our study, the gravity field perturbations cannot be represented by simple orbit perturbations without the accuracy loss.

We have evaluated orbit representation by means of Keplerian elements and Chebyshev polynomials, aiming to find the optimum compromise between message size and accuracy of the lunar orbiter navigation message.

Handling the Keplerian elements provides sufficient accuracy for the delivery of the broadcast ephemerides of the lunar orbiter. With a full 15-element RSW model, it is possible to obtain 95% of residuals of the orbital fit lower than 24 mm with the maximum value not exceeding 21 cm for a 1-hour orbit fit. It is recommended to use the full model considering 6 Keplerian and 9 empirical parameters.

To deliver the final position of the lunar orbiter, the Keplerian elements have to be transformed into the XYZ positions which are then corrected using numerical integration of the accelerations which are delivered as a set of empirical parameters. The accuracy of the lunar orbiter positions when using a fixed number of bits does not exceed 67, 694, 537, and 9065 mm for 1h, 1.5h, 2h, and 4h time windows, (95% of cases). Concerning the number of bits needed for the storage of the navigation message, for each time-window the number of bits is the same for both Keplerian elements and empirical accelerations regardless of the time window. The model requires 370 bits, another 14 are needed to mark the time stamp of the message, giving a total 401 bits.

To deliver a reliable navigation message which consider Keplerian elements and RSW accelerations, the numerical integration has to be conducted in the consistent force model and has to be delivered in the user environment. All this introduces the complexity of calculations, and the necessity of the implementation of the least-squares co-location, or different methods of numerical integration in the user's receiver. This significantly limits the optimization of the solution. For these reasons, a representation based on Keplerian elements is not recommended.

The second approach considered the orbit representation using Chebyshev polynomials. Several tests have been carried out to find the optimum trade-off between the accuracy of the orbit representation and the size of the message. The variable parameters considered include the window length, the degree of the Chebyshev polynomial, and the choice of scaling factor for encoding the coefficients from floating-point numbers to bits. The final recommendation is to use the division of the orbit into 1h windows and the fitting of a Chebyshev polynomial of degree 10 consisting of 11 coefficients. The scale factor of 2^{-5} should be used for all Chebyshev coefficients to obtain the orbit fit error at the centimeter level. The 95th percentile of the position error is up to 11 cm and the maximum residuals do not exceed 55 cm. The storage requirements for the individual coefficients are up to 197 bits per coordinate. In total, at least 591 bits must be allocated in the navigation message for each satellite.

In addition, the strategy can be modified to search for longer windows of validity of the Chebyshev polynomial or savings in bit allocation. The validity time of the proposed orbit model representation can be extended outside periselene. With the orbit representation using the Chebyshev polynomials composed of 11 coefficients (for each of the X, Y, and Z components), the validity time is useful during 1h and 2.5h windows, for periselene passes and outside periselene passes, respectively. In the analysis, the periselene passes have been identified based on the change in the satellite velocity. The change of the Chebyshev function validity time from 2.5h to 1h has been set up once the satellite velocity exceeds 1000 m/s inside the window.

It should be noted that the navigation message window length is shorter than the possible gap in the event of loss of communication between the satellite and the ground segment, which can be up to 8h. Navigation messages should therefore be prepared in advance by dividing the predicted orbit into windows of the recommended length, i.e. 1 hour, and transmitted to the satellite in batches. The batch should ensure uninterrupted system operation for at least the next 8 hours, so the batch consisting of the next 8 navigation messages should be transmitted in advance. It is also stressed that it is pointless to send Chebyshev polynomials representing velocities. The satellite velocities can be calculated based on the positions delivered to the users in the form of Chebyshev polynomials (see next section). We assessed the accuracy of such a method, and the accuracy of the velocity reconstruction is consistently below 30 mm/s, and below 3.5 mm/s for 95% of cases when considering Chebyshev polynomials composed of 11 coefficients. For lunar orbiters, the velocity error of 4 mm/s corresponds to a maximum error of the Doppler shift of df/f=2x10^{-11} of the relative frequency change (calculated as: $\frac{df}{f} = -\frac{1}{c}\frac{\Delta \boldsymbol{x} \circ \Delta \boldsymbol{v}}{|\Delta \boldsymbol{x}|}$).

The complete navigation message contains also other elements, which have not been discussed in the study, including clocks, health status, Signal-In-Space-Error, Issue-of-data identifier, time stamp, LST-UTC conversion parameters, and other data linked to auxiliary services (e.g. GNSS long-term ephemeris, the health status of other services, SAR data, Alert feed) and data in support to communication services. These aspects are contemplated in the Moonlight Navigation Signal in Space ICD – Navigation message.

Finally, a proposal for almanac data and the user algorithms for both Keplerian elements and Chebyshev polynomials have been provided.

9 CRITICAL ELEMENTS AND TECHNOLOGY ROADMAP

Although all technologies are mature and all building blocks are already available or can predate amply on the IDST and proximity link transceiver for the Lunar Gateway (especially for the digital processing modules), spread spectrum communications have never been used in deep space missions. On the other hand, spread spectrum/CDMA communications are the unavoidable backbone of the LRNS, independently of the adopted architecture. The lowest TRL are found for the onboard transceivers and the back-end ground receivers. Efficient and high-performance CDMA transceivers need to be developed. We suggest using a scaled down version of the transceiver developed at the level of elegant breadboard for the for the STE-QUEST mission. It is recommended to consider a scaled-down version of that transceiver for use onboard. For the ground CDMA receiver, the breadboard developed at ESOC needs to be beefed up by supporting higher chip rates. A CDM-M modulator needs to be developed in the uplink chain.

TABLE 6 TRL, with Comments, of the Critical Elements of the System

Item	TRL	Comment
GROUND		
Ground antennas+feed	7	Wide commercial availability for small diameter antennas (0.65m). Specific design is not yet available.
Ground X band amplifier	9	Solid state amplifier at 7.2 GHz with the required ADEV are widely available.
Ground K band amplifier	9	Solid state amplifiers at 23 GHz with the required ADEV are available. ESA has developed a 500 W SSA at 34 GHz (100 W already available ad DSA-3).
Ground modulator	5	A CDM-M modulator is required (TRL 5) for the ATLAS concept
Front-end receiver (K band)	9	Already in use in Europe. Svalbard antenna, 6.4 m in diameter, has tested K-band downlink capabilities with commercial satellites.

Ground back-end receiver	4	Breadboard under development at ESOC [RD52]
Range delay calibration system	5	Available at DSA-3 for Ka/Ka links. Easily adapted at K band.
Ionosphere cal system	8	GNSS calibration system already available. Only adaptations for near real time operations required.
Troposphere cal system	9	Water vapour radiometer calibrations already proven. Only required for precise wet tropospheric noise calibration
SPACE		
X band transceiver/transponder	4	Must support CDMA in addition to standard TT&C for S/C emergencies. Note that units are identical for both architectures (as for K band).
K band transceiver/transponder	5	Under development at TASI for Lunar Gateway proximity link. Hybrids for receiver and transmitter need to be modified because of slightly different frequencies.
Transceiver range delay calibration system	5	Available for the BepiColombo and JUICE KaT transponder
X band SSA amplifier	9	Space qualified units available
K band SSA amplifier	9	Space qualified units available
Onboard clock	9 (5)	USO or RAFS already available. Must be used for direct code epoch time tagging at the transceiver (not by the onboard computer). miniRAFS TRL based on private communication (P. Giordano). Safran miniRAFS online datasheet indicates that the unit is space qualified.
Signal Generation Unit	4	No critical technology envisaged. Individual components have likely TRL 9 (or slightly below). Low overall TRL is attributed because specific and detailed design is not yet available.

10 FINAL REMARKS

The proposed architecture of a lunar radio navigation system, consisting of four spacecraft in elliptical frozen orbits, was developed based on four key guidelines: simplification of the ground network, utilization of high Technology Readiness Level (TRL) hardware, cost-effective scalability to a larger constellation, and achieving excellent performance in orbit determination and time transfer. The adoption of the MSPA configuration for spacecraft tracking aligns with the goal of simplifying the ground system. This choice allows for the use of small antennas (less than 30 cm), which facilitates the deployment of network terminals and reduces the overall cost of the ground infrastructure. Furthermore, the small antenna size enables the design and assembly of compact and easily transportable terminals, enhancing the network's flexibility. To optimize cost and ease of deployment, it is advantageous for the LRNS backbone ground infrastructure to be in proximity to existing deep space tracking sites or radio astronomical antennas. These ground antennas already possess hydrogen maser frequency standards and fast communication lines, which are crucial to the overall system. One drawback of the proposed configuration is the requirement for small (30 cm) steerable antennas onboard the spacecraft. However, steerable antennas provide sufficient data rates for telecommands and telemetry, supporting the frequent upload of navigation messages and the download of housekeeping data and CE time-stamps. Thanks to nearly continuous visibility, the daily data volume achieved with the proposed architecture is comparable to that obtained with a much larger antenna (e.g., 10-15 m diameter) tracking the constellation's nodes sequentially. This further emphasizes the efficiency and practicality of the system design.

Most elements of the radio system have a high Technology Readiness Level (TRL) (> 5), despite the selection of K-band for the radio link. A notable exception is the CDMA back-end receiver, which is currently being developed at the breadboard level. This receiver is specifically designed to support spread spectrum (SS) signals with a bandwidth of 6 MHz. It is worth mentioning that CDMA/CDM-M modulations have not yet been used in deep space communications. Nonetheless, the existing digital transponders can be readily modified to meet the requirements of the proposed radio link configuration. In terms of passive elements, there are already commercially available, space-qualified, steerable antennas operating at K-band. These off-the-shelf antennas are fully compatible with an accommodation on small-sat and can be used effectively within the system.

Although the constellation considered for ESA's Moonlight initiative is designed to support missions in the southern polar regions of the Moon, the future of lunar exploration will certainly need an extended coverage and an increased number of spacecraft. The proposed architecture would make such an expansion straightforward. The ground support to an extended constellation requires only the deployment of additional ground terminals, each supporting a separate set of nodes. Key to expandability is the selection of K-band rather than X-band. Indeed, the much larger available bandwidth (500 MHz vs. 50 MHz) allows a much greater flexibility in the selection of the signal structure. The use of SS signals at large chip rates (24-25 Mcps in our concept), essential to attain good ranging accuracies (33 cm @ 10 s integration time), is possible only in K-band. In addition, K-band provides a much-improved immunity to charged particle effects in radio-metric measurements.

While ESA's Moonlight initiative initially focuses on supporting missions in the southern polar regions of the Moon, the future of lunar exploration will inevitably require expanded coverage and a larger number of spacecraft. The proposed architecture of the LRNS is designed to facilitate such expansion seamlessly. Expanding the constellation simply involves deploying additional ground terminals, each supporting a separate set of nodes. This scalability is a crucial advantage of the proposed architecture. The selection of K-band as the operating frequency is a key factor in enabling this expandability. Compared to X-band, K-band offers a significantly larger available bandwidth (500 MHz compared to 50 MHz), providing much greater flexibility in designing the signal structure. The utilization of spread spectrum (SS) signals at high chip rates (specifically 24-25 Mcps in this concept) is essential for achieving accurate ranging capabilities (33 cm accuracy with a 10-second integration time). Such high chip rates can only be implemented in the K-band. Furthermore, K-band exhibits improved immunity to charged particle effects in radio-metric measurements, making it advantageous for accurate and precise data acquisition. Therefore, by adopting K-band, the proposed architecture not only allows for straightforward expansion but also enhances the system's performance in terms of ranging accuracy and immunity to charged particle effects.

The proposed architecture, utilizing K-band and high chip rate spread spectrum (SS) signals, offers several advantages, including high precision and bias-free range and range rate measurements. Moreover, the adoption of the MSPA tracking configuration enables the inclusion of a third data type through SBI. Implementing SBI is straightforward, as it involves differencing the receiver phases from any pair of spacecraft without requiring additional hardware. The OD accuracy heavily relies on the quality of radio-metric measurements. Numerical simulations conducted on the proposed architecture demonstrate that the SISE consistently meets the Moonlight initiative's requirements. Additionally, the simulations show that the ephemerides' aging is gradual enough to necessitate uploading a new navigation message at intervals of several hours, ensuring reliable and up-to-date orbital data to the end user.

11 PERSONNEL AND ACKNOWLEDGMENTS

The ATLAS consortium relied on the contribution of many engineers and scientists from academic institutions and industries:

Luciano Iess (Study Lead), Mauro Di Benedetto (Deputy Study Lead), Giovanni Boscagli, Paolo Racioppa, Andrea Sesta, Fabrizio De Marchi, Paolo Cappuccio, Daniele Durante, Serena Molli, Michael K. Plumaris, and Pasquale Tartaglia, *Sapienza University of Rome, CRAS and Dept. of Mechanical and Aerospace Engineering, Rome (I)*

Debora Pastina and Fabrizio Santi, *Sapienza University of Rome, CRAS and Dept. of Information Engineering, Electronics and Telecommunication, Rome (I)*

Agnes Fienga GéoAzur, *CNRS, Observatoire de la Côte d'Azur, Valbonne (F)*

Nicolas Rambeaux, *IMCCE, CNRS, Paris (F)*

Krzysztof Sosnica, Grzegorz Bury, Radoslaw Zajdel, *Wrocław University of Environmental and Life Sciences, Wrocław, (PL)*

Nicola Linty and Carolina Molteni, *Argotec s.r.l., Turin (I)*

Jacopo Belfi, *Leonardo S.p.A, Nerviano (I)*

We wish to thank Pietro Giordano, Richard Swinden and Javier Ventura-Traveset for many suggestions and requests that helped us in delivering a more comprehensive and consistent output of the study.

12 REFERENCES

Asmar, S. W., Armstrong, J. W., Iess, L., & Tortora, P. (2005). Spacecraft Doppler tracking: Noise budget and accuracy achievable in precision radio science observations. *Radio Science*, *40*(2), 1-9.

Bauer, S. et al. (2017). Analysis of one-way laser ranging data to LRO, time transfer and clock characterization. *Icarus* 283, 38-54.

Bender, P. L. (1994). Proposed microwave transponders for early lunar robotic landers. *Advances in Space Research*, 14(6), 233-242.

Cappuccio, P., Notaro, V., di Ruscio, A., Iess, L., Genova, A., Durante, D., ... & Simone, L. (2020). Report on First Inflight Data of BepiColombo's Mercury Orbiter Radio Science Experiment. *IEEE Transactions on Aerospace and Electronic Systems*, *56*(6), 4984-4988.

Cappuccio, P., Hickey, A., Durante, D., Di Benedetto, M., Iess, L., De Marchi, F., ... & Mura, A. (2020). Ganymede's gravity, tides and rotational state from JUICE's 3GM experiment simulation. *Planetary and Space Science*, 187, 104902.

Consultative Committee for Space Data Systems (2021). Radio Frequency and Modulation System – Informational Report (Green Book). Issue 2, CCSDS 500.1-G-2.

Damour T, Soffel M, Xu C (1991) General-relativistic celestial mechanics. I. Method and definition of reference systems. *Phys. Rev. D* 43(10):3273–3307, DOI 10.1103/PhysRevD.43.3273

Delva, P., Meynadier, F., Le Poncin-Lafitte, C., Laurent, P., & Wolf, P. (2012, April). Time and frequency transfer with a microwave link in the ACES/PHARAO mission. In *2012 European Frequency and Time Forum* (pp. 28-35). IEEE.

Donà, G. & Iess, L. (2017, March). CDMA Implementation for TT&C and Precision Navigation - Scenario Analysis and Signal Definition. *Technical note TN-002-1*, Thales Alenia Space Italia, ESA Contract No. 4000117076/16/NL/FE.

Duchayne, L., Mercier, F., & Wolf, P. (2009). Orbit determination for next generation space clocks. *Astronomy & Astrophysics*, *504*(2), 653-661.

Gregnanin, M., Bertotti, B., Chersich, M., Fermi, M., Iess, L., Simone, L., ... & Williams, J. G. (2012). Same beam interferometry as a tool for the investigation of the lunar interior. *Planetary and Space Science*, *74*(1), 194-201.

Gregnanin, M., Yseboodt, M., Dehant, V., Iess, L., & Van Hoolst, T. (2014, April). Estimation of Mars geophysical information through Same Beam Interferometry. In *Proc. European Planetary Science Congress* EPSC 2014.

Howe, D. A., Hanson, D. W., Jesperscn, J. L., & Lombardi, M. A. (1989, November). Satellite two-way time transfer: Fundamentals and recent progress. In *Proceedings of the 21th Annual Precise Time and Time Interval Systems and Applications Meeting*, 117-130.

Iess, L., Di Benedetto, M., James, N., Mercolino, M., Simone, L., & Tortora, P. (2014). Astra: Interdisciplinary study on enhancement of the end-to-end accuracy for spacecraft tracking techniques. *Acta Astronautica*, 94(2), 699-707.

Iess, L., Folkner, W. M., Durante, D., Parisi, M., Kaspi, Y., Galanti, E., ... & Bolton, S. J. (2018). Measurement of Jupiter's asymmetric gravity field. *Nature*, *555*(7695), 220-222.

ITU-R TF.1153-4. (2015, August) . The operational use of two-way satellite and frequency transfer employing pseudorandom noise codes' Time signals and frequency standards emissions. https://www.itu.int/dms_pubrec/itu-r/rec/tf/R-REC-TF.1153-4-201508-I!!PDF-E.pdf

Manghi, R. L., Bernacchia, D., Casajus, L. G., Zannoni, M., Tortora, P., Martellucci, A., ... & Iess, L. (2023). Tropospheric delay calibration system performance during the first two BepiColombo solar conjunctions. *Radio Science*, *58*(2), 1-15.

Moyer, T. (2003). Formulation for Observed and Computed Values of Deep Space Network Data Types for Navigation, 576 pp., John-Wiley & Sons. (Also available at https://descanso.jpl.nasa.gov/monograph/series2/Descanso2_all.pdf)

Simone, L., Fittipaldi, G., et al. (2010, September). Techniques to increase the secure TT&C anti jamming capabilities beyond the processing gain. *Proceedings of TTC 2010 5th ESA International Workshop on Tracking, Telemetry and Command Systems for Space Applications*.